Cell. Mol. Life Sci. (2014) 71:2731–2745
DOI 10.1007/s00018-013-1525-8

Cellular and Molecular Life Sciences

RESEARCH ARTICLE

Inhibition of Ku70 acetylation by INHAT subunit SET/TAF-Iβ regulates Ku70-mediated DNA damage response

Kee-Beom Kim · Dong-Wook Kim · Jin Woo Park · Young-Joo Jeon · Daehwan Kim · Sangmyung Rhee · Jung-Il Chae · Sang-Beom Seo

Received: 16 August 2013 / Revised: 28 October 2013 / Accepted: 14 November 2013 / Published online: 5 December 2013

Abstract DNA double-strand breaks (DSBs) can cause either cell death or genomic instability. The Ku heterodimer Ku70/80 is required for the NHEJ (non-homologous end-joining) DNA DSB repair pathway. The INHAT (inhibitor of histone acetyltransferases) complex subunit, SET/TAF-Iβ, can inhibit p300- and PCAF-mediated acetylation of both histone and p53, thereby repressing general transcription and that of p53 target genes. Here, we show that SET/TAF-Iβ interacts with Ku70/80, and that this interaction inhibits CBP- and PCAF-mediated Ku70 acetylation in an INHAT domain-dependent manner. Notably, DNA damage by UV disrupted the interaction between SET/TAF-Iβ and Ku70. Furthermore, we demonstrate that overexpressed SET/TAF-Iβ inhibits recruitment of Ku70/80 to DNA damage sites. We propose that dysregulation of SET/TAF-Iβ expression prevents repair of damaged DNA and also contributes to cellular proliferation. All together, our findings indicate that SET/TAF-Iβ interacts with Ku70/80 in the nucleus and inhibits Ku70 acetylation. Upon DNA damage, SET/TAF-Iβ dissociates from the Ku complex and releases Ku70/Ku80, which are then recruited to DNA DSB sites via the NHEJ DNA repair pathway.

Keywords SET/TAF-Iβ · Ku70 · Ku80 · Acetylation · DNA damage response

Electronic supplementary material The online version of this article (doi:10.1007/s00018-013-1525-8) contains supplementary material, which is available to authorized users.

K.-B. Kim · J. W. Park · D. Kim · S. Rhee · S.-B. Seo (✉)
Department of Life Science, College of Natural Sciences, Chung-Ang University, Seoul 156-756, Republic of Korea
e-mail: sangbs@cau.ac.kr

D.-W. Kim · Y.-J. Jeon · J.-I. Chae (✉)
Department of Oral Pharmacology, School of Dentistry, Brain Korea 21 PLUS Project, Chonbuk National University, Jeonju 561-756, Republic of Korea
e-mail: jichae@chonbuk.ac.kr

Present Address:
D.-W. Kim
Department of Microbiology, Immunology, and Cancer Biology, School of Medicine, University of Virginia, Charlottesville, VA, USA

Introduction

DNA DSBs (double-strand breaks) can be introduced by exogenous agents, including UV irradiation. Unrepaired DSBs can lead to genomic instability and malignant transformation [1]. In mammalian cells, DSBs are repaired by two major pathways: homologous recombination (HR) and nonhomologous end joining (NHEJ) [2]. The initial step of NHEJ is the detection and binding of the Ku70/80 heterodimer to the ends of DSBs. Upon binding to DNA, Ku recruits other factors required for NHEJ, including DNA-dependent protein kinase catalytic subunits (DNA-PKcs), XRCC4, ligase IV, XLF, and Artemis [2]. Ku70 and Ku80 are known to undergo posttranslational modification; lysine residues (K317, K331, K338, K539, K542, K544, K553, and K556) of Ku70 are targeted for acetylation by CBP and PCAF. Acetylation of the Ku70 C-terminal linker domain inhibits the ability of Ku70 to suppress Bax-mediated apoptosis [3]. SIRT1 deacetylates Ku70, causing it to sequester the proapoptotic factor Bax away from mitochondria, thereby inhibiting stress-induced apoptotic cell death [4]. Upon treatment with the HDAC inhibitor TSA, acetylated Ku70 releases Bax, which then translocates to mitochondria and triggers cytochrome *c* release, resulting in caspase-dependent death [5]. HDAC inhibitors have also

been reported to induce Ku70 acetylation, thereby diminishing the ability of Ku70 to repair DNA damage [6].

We previously identified SET/TAF-Iβ and pp32 as subunits of the INHAT complex demonstrating high affinity for histones; consequently, binding of these proteins to histones prevents histone acetylation by p300/CBP and PCAF and thereby represses transcription of target genes [7, 8]. INHAT is a multiprotein complex composed of highly acidic domain-containing proteins SET/TAF-Iβ, TAF-Iα, and pp32 [8]. As multitasking proteins, SET/TAF-Iβ and pp32 have been reported to be negative and positive regulators of caspase-independent and -dependent apoptotic signaling, respectively [9–11]. Moreover, SET/TAF-Iβ was originally identified as a translocated gene in acute undifferentiated leukemia, a finding which further supports its oncogenic activity [12–14]. We also reported that SET/TAF-Iβ inhibits p53 acetylation and blocks both p53-mediated cell cycle arrest and apoptosis in response to cellular stress via repression of transcription of p53 target genes [15].

In this study, we investigated the role of SET/TAF-Iβ in Ku70/80-mediated NHEJ DNA repair. We demonstrate that SET/TAF-Iβ interacts with Ku70/80 in vivo and inhibits Ku70 acetylation by CBP and PCAF in an INHAT domain-dependent manner. Moreover, we show that this interaction is disrupted by DNA damage. Our data support a model in which Ku70/80 proteins interact with SET/TAF-Iβ in the normal cellular environment; once DNA damage is introduced, Ku proteins are recruited to DNA damage sites upon dissociation from SET/TAF-Iβ. Association with and dissociation from Ku proteins did not occur with the INHAT domain-deleted SET/TAF-IβΔC5 truncation, suggesting that inhibition of Ku acetylation plays an important role in this mechanism.

Materials and methods

Two-dimensional electrophoresis analysis

To identify interacting partners of SET/TAF-Iβ, we employed 2-DE analysis comprising both isoelectric focusing (IEF) (first dimension) and SDS-PAGE (second dimension). Briefly, the TAP-SET/TAF-Iβ complex and its associated binding partners were eluted from beads with 200 μl of rehydration solution (7 M urea, 2 M thiourea, 4 % (wt/vol) CHAPS, 18 mM DTT, and a trace amount of Bromophenol blue). The first dimension (IEF) was carried out using an IPGphor unit (Amersham Biosciences) with pre-cast nonlinear IPG gel strips (18 cm, pH 3–11; Amersham Biosciences). The equilibrated IPG gel strips were loaded on 12 % SDS-PAGE gels for the second dimension separation, performed by using a Protean II xi 2-DE cell (Bio-Rad) at 20 mA. The procedure was independently repeated at least three times to ensure reproducibility.

In-gel protein digestion

Separated 2-DE gels were visualized using a PlusOne Silver Staining Kit (Amersham Biosciences) according to the manufacturer's protocol. After electrical scanning and analysis of silver-stained gels using Phoretix Expression software ver. 2005 (Nonlinear Dynamics), the protein bands of interest were excised and digested in-gel with sequencing-grade modified trypsin (Promega, Madison, WI, USA), as previously described [16]. Briefly, excised protein bands were washed with a 1:1 mixture of acetonitrile and 25 mM ammonium bicarbonate (pH 7.8), and subsequently dried using a Speedvac concentrator. After drying, rehydration was performed with 25 mM ammonium bicarbonate (pH 7.8) and trypsin. Tryptic peptides were then extracted from supernatants with a 50 % aqueous acetonitrile solution containing 0.1 % formic acid. After preparation, tryptic peptides were then analyzed using reversed-phase capillary HPLC directly coupled to a Finnigan LCQ ion trap mass spectrometer (LC–MS/MS), as previously described [17].

LC–MS/MS

Three extractions were performed to recover all tryptic peptides from the gel slices. Recovered peptides were then concentrated by drying the combined extracts in a vacuum centrifuge. Concentrated peptides were then mixed with 20 μl of 0.1 % formic acid in 3 % acetonitrile in preparation for LC–MS/MS analysis. Nano LC of the tryptic peptides was performed using the Waters Nano LC system equipped with a Waters C18 nano column (75 μm × 15 cm nanoAcquity UPLC column). Binary solvent A1 contained 0.1 % formic acid in water, and binary solvent B1 contained 0.1 % formic acid in acetonitrile. Samples (5 μl) were loaded onto the column, and peptides were subsequently eluted with a binary solvent B1 gradient (2–40 %, 30 min, 0.4 μl/min). The lock mass, [Glu1] fibrinopeptide at 400 fmol/μl, was delivered from the auxiliary pump of the Nano LC system at 0.3 μl/min to the reference sprayer of the NanoLockSpray source.

Data processing and protein identification

For tandem mass spectrometry, LC–MS/MS data were processed and used in database searches using the PLGS (Protein Lynx Global Server) version 2.4 (Waters). Spectra were automatically smoothed, background-subtracted, centered, and de-isotoped with the automatic tolerance settings. In addition, charge states were reduced, and masses

were corrected based on reference scans. Ion detection, clustering, and normalization were performed using PLGS. Processed ions were sequenced and mapped against the NCBI human database using the PLGS and Mascot Daemon programs (http://www.matrixscience.com).

Plasmids

The pCMX-SET/TAF-Iβ plasmid was previously described [8]. Both pOTB7-Ku70 (BC010034) and -Ku80 (BC019027) were purchased from KUGI. The Ku70 and Ku80 coding sequences were subcloned into the bacterial expression vector pGEX-4T1 (Amersham Biosciences), thereby generating constructs for the production of glutathione *S*-transferase (GST)-tagged fusion proteins. To construct mammalian expression vectors for the production of HA-, myc-, and His-tagged Ku70; GFP-tagged Ku70; and Flag-tagged Ku80, pcDNA6-HA-myc-his (Invitrogen), pEGFP-C1 (Clontech), and p3XFlag-CMV-10 (Sigma) were used, respectively. The pNTAP-B expression vector (Stratagene) was modified to generate pNTAP-SET/TAF-Iβ, used for the production of streptavidin- and calmodulin-binding peptide-tagged SET/TAF-Iβ. The plasmid expressing shRNA directed against human SET/TAF-Iβ (RHS4533) was purchased from Open Biosystems.

Antibodies

Antibodies against SET/TAF-Iβ (sc-25564), Ku70 (sc-55505), Ku80 (sc-5280), GST (sc-138), HA (Y-11, sc-805), p53 (DO-1, sc-126) acetyl-lysine (Ac–K, sc-32268), GFP (sc-9996), histone H3 (sc-8654), β-actin (sc-47778, Santa Cruz Biotechnology), the calmodulin-binding epitope (07-482), acetyl-p53 (K320, 06-915), H2AX (Ser139, 05-636, Millipore), Flag (F3165, Sigma), and β-tubulin (#2146, Cell Signaling) were employed for immunoblot, immunoprecipitation, and chromatin immunoprecipitation (ChIP) analyses.

Tandem affinity purification

Tandem affinity purification (TAP) was essentially conducted as previously described [18], except that an InterPlay mammalian TAP system (Stratagene) was used. After the two-step purification, protein eluates were subjected to protease digestion, followed by LC–MS/MS analysis.

Immunoprecipitation

For the Ku70/80 and SET/TAF-Iβ binding assays, transfected cells were lysed in RIPA buffer [50 mM Tris–HCl (pH 8.0), 150 mM NaCl, 0.1 % SDS, 0.5 % SDC, 1 % NP-40, 1X protease inhibitor cocktail, and 1 mM EDTA] and immunoprecipitated with anti-SET/TAF-Iβ or anti-GFP antibodies in IP buffer [50 mM Tris–HCl (pH 7.5), 150 mM NaCl, 1 mM EDTA, 1 mM EGTA, 1 % Triton X-100, 1 mM PMSF, and 1X protease inhibitor cocktail] overnight at 4 °C. Protein A/G agarose beads (GenDEPOT) were then added for 2 h with agitation at 4 °C. Bound proteins were eluted and analyzed by immunoblotting with anti-SET/TAF-Iβ, anti-GFP, and anti-Flag antibodies.

In vitro INHAT assay

INHAT assays were carried out by incubating 20–30 pmol of purified GST-SET/TAF-Iβ with 1 μg of GST-Ku70 in 5X HAT buffer [250 mM Tris–HCl (pH 8.0), 50 % glycerol, 0.5 mM EDTA, 5 mM dithiothreitol, 0.5 mM PMSF, and 50 mM sodium butyrate] [8] for 30 min on ice. Following pre-incubation, 1 pmol of PCAF or 1 μg of CBP, along with ^{14}[C]-acetyl CoA (50 μCi/μl, Perkin Elmer), was added. Reactions were then incubated for 2 h at 30 °C. Reaction complexes were separated by SDS-PAGE and analyzed with a phosphorimager. For scintillation counting, Ku70 (537–546) peptides [EGKVTKRKHD] were synthesized (Peptron) based on the N-terminal amino acid sequence of histone H3. Peptides were filtered with p81 filter paper (Millipore) and washed three times with cold 10 % TCA and 70 % ethanol for 5 min at RT. Filters were then allowed to air dry, followed by the addition of 1 ml of Ultima Gold (Perkin Elmer). ^{14}[C]-acetyl CoA was ultimately quantified with a scintillation counter.

Chromatin immunoprecipitation (ChIP) assay and real-time PCR

ChIP was carried out as described in the protocols from Millipore. Briefly, 293TdA3-stable cells were transfected with *I-Sce*I endonuclease and harvested 48 h later. Proteins were cross-linked by the addition of 1 % formaldehyde to the medium and incubated for 10 min. After cross-linking, 125 mM glycine was added at room temperature, followed by incubation for 5 min; cells were then scraped into SDS lysis buffer. Samples were further sonicated and diluted for immunoprecipitation in dilution buffer [0.01 % SDS, 1.1 % Triton X-100, 1.2 mM EDTA, 16.7 mM Tris–HCl (pH 8.1), and 167 mM NaCl] with antibodies against Flag, HA, phosho-H2AX, and IgG. Immunoprecipitated complexes were recovered with protein A/G-agarose beads (GeneDEPOT). After reversing the cross-links, chromatin was subjected to proteinase K digestion, and DNA was purified for PCR amplification using a PCR purification kit (QIAGEN). To analyze the damaged regions of DNA, primer sets consisting of 0.3-kb regions (sense, 5′-ATGGGCTACGGCTTCTACCA-3′; antisense, 5′-GCCGTCCTCGTACTTCTCGAT-3′), 1.2-kb regions (sense, 5′-GGTGTGCGTTTGTCTATATGTGATT-3′;

antisense, 5′-CCTAGGAATGCTCGTCAAGAAGA-3′), and 2.5-kb regions (sense, 5′-CCCTGAACCTGAAACA TAAAATGA-3′; antisense, 5′-TGTGAAATTTGTGATG CTATTGCTT-3′) were used. The amplification reaction was performed using 45 cycles of the following conditions: denaturation at 94 °C, annealing at 58 °C, and extension at 72 °C. Disassociation curves were generated after each PCR run to ensure that a single product of appropriate length was amplified. The mean $C_t \pm$ SE was calculated from individual C_t values, obtained from triplicate determinations per stage. The normalized mean C_t was estimated as ΔC_t by subtracting the mean C_t of input from that of the individual region.

NHEJ assay

pIRES-TK-EGFP DNA was transfected into 293T cells using Lipofectamine 2000 (Invitrogen), and 293TdA3 cells stably expressing TK-EGFP were obtained through puromycin selection (2 μg/ml) [19]. pCBASce DNA (1 μg) was transfected into 293TdA3 stable cells in a 24-well plate (7.5×10^4 cells/well) with Lipofectamine 2000. For quantification of GFP-tagged protein levels, cells were harvested by trypsinization, washed with phosphate-buffered saline, lysed in RIPA buffer, and ELISA assays were performed. To quantify both uncut and joined DNA, genomic DNA was purified from cells and 20 ng of DNA was analyzed by real-time PCR. Two-step PCR was performed for 45 cycles, consisting of denaturation at 95 °C for 30 s and annealing and extension at 60 °C for 60 s, using the CFX 96 Real-Time System (Bio-Rad). β-actin DNA was co-amplified and quantified as an internal control. Similar proportions of uncut DNA (reflecting the efficiency of *I-Sce*I digestion) were reproducibly observed, regardless of the expression levels of SET/TAF-Iβ, SET/TAF-IβΔC5, or shRNA directed against SET/TAF-Iβ. To examine the effects of SET/TAF-Iβ on DNA joining, cells were subjected to the NHEJ assay and immunoblot analysis 48 h after transfection of the indicated constructs. To evaluate the amounts of uncut and joined DNA, primer sets specific for uncut (sense, 5′- CGTTTGCCCGGGAGATG-3′; antisense, 5′- CGACCGGTAGGCGTTATCAG-3′), joined (sense, 5′- CGTACGTCTCCGGATTCGAA-3′; antisense, 5′- GTGATGCGGCACTCGATCTT-3′), and internal control DNA (sense, 5′- TTTACCGGCTACTTGCCAAT-3′; antisense, 5′- GAAAGCTGTCCCCAGTCCT-3′) were used.

Results

Inhibition of Ku70 acetylation by SET/TAF-Iβ

A previous report found that acetylation of Ku70 by CBP and PCAF at its C-terminal linker domain disrupts Bax interaction, thereby resulting in apoptotic cell death [3]. To better understand the mechanisms by which Ku acetylation is regulated, we hypothesized that the INHAT domain of SET/TAF-Iβ inhibits acetylation of Ku proteins by both CBP and PCAF. We began by performing in vitro HAT assays with recombinant PCAF, CBP, and Ku70, and confirmed that PCAF and CBP both acetylated Ku70, consistent with previous reports (Fig. 1a, b). Furthermore, the addition of increasing amounts of SET/TAF-Iβ to the reactions induced fivefold and fourfold decreases in PCAF- and CBP-mediated Ku70 acetylation, respectively (Fig. 1a, b). Using the C-terminal INHAT domain-deleted mutant, SET/TAF-IβΔC3, we verified that the INHAT domain is required for SET/TAF-Iβ-mediated inhibition of PCAF- and CBP-mediated Ku70 acetylation (Fig. 1a, b). Inhibition of Ku70 acetylation by SET/TAF-Iβ was further confirmed in vivo by immunoprecipitation of Ku70. In transiently co-transfected 293T cells, high levels of Ku70 acetylation by PCAF and CBP were observed (Fig. 1c, d). As expected, overexpression of SET/TAF-Iβ inhibited Ku70 acetylation (Fig. 1c, d). However, deletion of the C-terminal region of SET/TAF-Iβ (SET/TAF-IβΔC3) rendered it unable to inhibit Ku70 acetylation (Fig. 1c, d). This observation implies that acetylation of Ku70 is mediated by the acidic C-terminus of the INHAT domain of SET/TAF-Iβ. Furthermore, shRNA-mediated knockdown of SET/TAF-Iβ resulted in increased acetylation of ectopically expressed GFP-Ku70, indicating that SET/TAF-Iβ

Fig. 1 SET/TAF-Iβ inhibits PCAF- and CBP-mediated Ku70 acetylation. **a**, **b** Acetylation assays of Ku70 with PCAF and CBP were performed with increasing concentrations of SET/TAF-Iβ or SET/TAF-IβΔC3. Autoradiograms of INHAT assays using recombinant **a** PCAF or **b** CBP with SET/TAF-Iβ, SET/TAF-IβΔC3, and GST-Ku70 (*top*), followed by Coomassie staining (*bottom*). The *numbers below the phosphor images* represent quantifications of the levels of Ku70 acetylation. **c**, **d** 293T cells were transfected with various plasmids as indicated. After anti-GFP (Ku70) immunoprecipitations, eluted proteins were subjected to Western blotting with anti-acetyl-lysine antibodies. The amounts of immunoprecipitated SET/TAF-Iβ were determined by Western blotting, and are shown in the *lower panels*. Quantifications of the band intensities of acetylated Ku70 are shown below. **e**, **f** Stable SET/TAF-Iβ knockdown cells were transfected with constructs driving the expression of GFP-Ku70 and HATs (PCAF or CBP). Cell lysates were immunoprecipitated with anti-GFP antibodies; eluates were then immunoblotted with anti-acetyl-lysine, anti-GFP, and anti-SET/TAF-Iβ antibodies. **g** Nuclear extracts prepared from stable SET/TAF-Iβ knockdown cells were subjected to immunoprecipitation with anti-Ku70 antibodies. Ku70 complexes were then immunoblotted with anti-acetyl-lysine antibodies. **h**, **i** Ku70 peptides (537–546) were used as substrates in INHAT assays with (**h**) PCAF or (**i**) CBP, GST-SET/TAF-Iβ, and GST-SET/TAF-IβΔC3. Acetylation levels were quantified via filter binding assays and are represented as raw counts per minute (*cpm*), as determined by scintillation counting. Data shown represent averages of three independent experiments, with *error bars* representing ± SDs

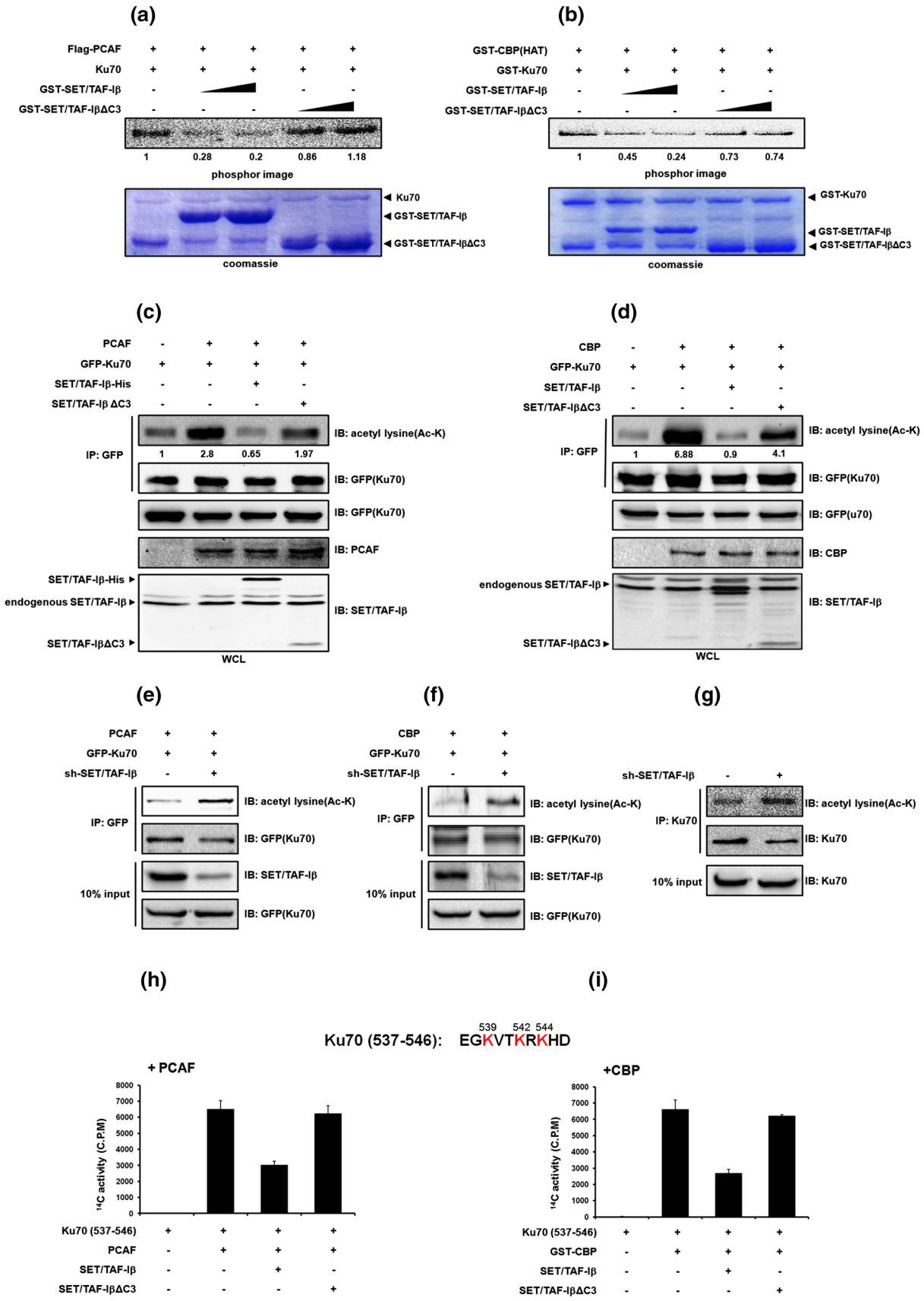
(a)
Flag-PCAF + + + + +
Ku70 + + + + +
GST-SET/TAF-Iβ - - -
GST-SET/TAF-IβΔC3 - - -
1 0.28 0.2 0.86 1.18
phosphor image
Ku70
GST-SET/TAF-Iβ
GST-SET/TAF-IβΔC3
coomassie
(b)
GST-CBP(HAT) + + + + +
GST-Ku70 + + + + +
GST-SET/TAF-Iβ - - -
GST-SET/TAF-IβΔC3 - - -
1 0.45 0.24 0.73 0.74
phosphor image
GST-Ku70
GST-SET/TAF-Iβ
GST-SET/TAF-IβΔC3
coomassie
(c)
PCAF - + + +
GFP-Ku70 + + + +
SET/TAF-Iβ-His - - + -
SET/TAF-Iβ ΔC3 - - - +
IP: GFP
1 2.8 0.65 1.97
IB: acetyl lysine(Ac-K)
IB: GFP(Ku70)
IB: GFP(Ku70)
IB: PCAF
SET/TAF-Iβ-His
endogenous SET/TAF-Iβ
SET/TAF-IβΔC3
IB: SET/TAF-Iβ
WCL
(d)
CBP - + + +
GFP-Ku70 + + + +
SET/TAF-Iβ - - + -
SET/TAF-IβΔC3 - - - +
IP: GFP
1 6.88 0.9 4.1
IB: acetyl lysine(Ac-K)
IB: GFP(Ku70)
IB: GFP(u70)
IB: CBP
endogenous SET/TAF-Iβ
SET/TAF-IβΔC3
IB: SET/TAF-Iβ
WCL
(e)
PCAF + +
GFP-Ku70 + +
sh-SET/TAF-Iβ - +
IP: GFP
IB: acetyl lysine(Ac-K)
IB: GFP(Ku70)
10% input
IB: SET/TAF-Iβ
IB: GFP(Ku70)
(f)
CBP + +
GFP-Ku70 + +
sh-SET/TAF-Iβ - +
IP: GFP
IB: acetyl lysine(Ac-K)
IB: GFP(Ku70)
10% input
IB: SET/TAF-Iβ
IB: GFP(Ku70)
(g)
sh-SET/TAF-Iβ - +
IP: Ku70
IB: acetyl lysine(Ac-K)
IB: Ku70
10% input
IB: Ku70
(h)
+ PCAF
14C activity (C.P.M)
8000 7000 6000 5000 4000 3000 2000 1000 0
Ku70 (537-546) + + + +
PCAF - + + +
SET/TAF-Iβ - - + -
SET/TAF-IβΔC3 - - - +
(i)
539 542 544
Ku70 (537-546): EGKVTKRKHD
+CBP
14C activity (C.P.M)
8000 7000 6000 5000 4000 3000 2000 1000 0
Ku70 (537-546) + + + +
GST-CBP - + + +
SET/TAF-Iβ - - + -
SET/TAF-IβΔC3 - - - +

inhibits PCAF- and CBP-mediated Ku70 acetylation (Fig. 1e, f). Moreover, shRNA-mediated knockdown of SET/TAF-Iβ also resulted in increased acetylation of nuclear-resident, endogenous Ku70, thereby confirming that endogenous SET/TAF-Iβ inhibits Ku70 acetylation in the nucleus (Fig. 1g). As a complementary approach to confirm the ability of SET/TAF-Iβ to inhibit Ku70 acetylation, we conducted INHAT assays with Ku70 peptides, containing three lysine residues independently targeted for acetylation, and measured their acetylation levels [3]. Incubation of Ku70 (537–546) peptides with CBP and PCAF resulted in high levels of acetylation. Furthermore, the addition of SET/TAF-Iβ, but not SET/TAF-IβΔC3, significantly reduced the levels of Ku70-peptide acetylation, thereby confirming that SET/TAF-Iβ exerts INHAT activity on the non-histone protein, Ku70 (Fig. 1h, i).

Tandem affinity purification of SET/TAF-Iβ-interacting proteins

To identify interacting partners of SET/TAF-Iβ in vivo, we generated a construct driving the expression of calmodulin-streptavidin-tagged SET/TAF-Iβ, which was then introduced into HeLa cells. SET/TAF-Iβ-interacting proteins, present in SET/TAF-Iβ complexes, were purified by tandem affinity purification (TAP) using both streptavidin- and calmodulin-binding resins (Fig. 2a). Proteins associated with SET/TAF-Iβ were then resolved by two-dimensional electrophoresis (2-DE) and visualized by silver staining. Several spots appeared on the gel in which protein extracts of cells expressing TAP-SET/TAF-Iβ were separated (Supplementary Fig. S1). Spots that were differentially present between the mock and TAP-SET/TAF-Iβ purifications

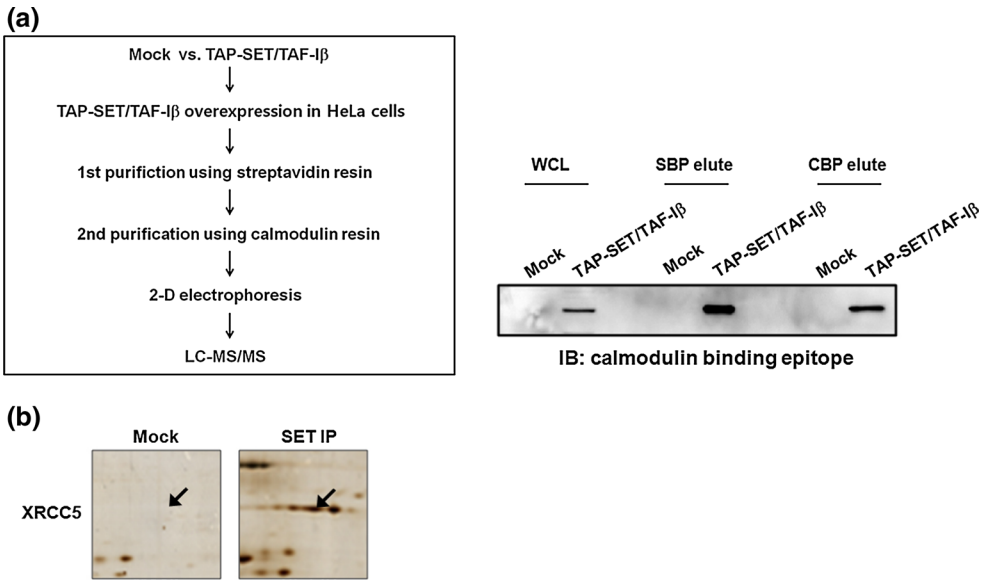

Fig. 2 2-DE gel electrophoresis. **a** Schematic representation of TAP-SET/TAF-Iβ. *Left panel*: Workflow of process for obtaining TAP-SET/TAF-Iβ complexes. *Right panel*: Verification of mock (empty vector) and TAP-SET/TAF-Iβ-expressing HeLa cells by Western blotting of cellular lysates with anti-calmodulin antibodies. **b** Enlarged image of the XRCC5 spot in a control 2-DE gel, compared to the corresponding spot in a 2-DE gel from the TAP-SET/TAF-Iβ sample. For the detailed protocol, see "Materials and methods"

Table 1 Proteins differentially identified in cells overexpressing SET/TAF-Iβ compared to control cells

Spot no.	Accession no.	Identified proteins	SwissProt no.	UniGene no.	Symbol	Sequence coverage (%)	Matched peptide	Pi	Mass (Da)	Score
1	gil5453740	Myosin regulatory light chain 12 A	P19105	Hs. 190086	MYL12A	5	1	4.67	19,752	48
2	gil5453740	Myosin regulatory light chain 12 A	P19105	Hs. 190086	MYL12A	12	2	4.67	19,752	71
3	gil10863945	X-ray repair cross-complementing protein 5	P13010	Hs.388739	XRCC5	29	31	5.55	83,222	723
4	gil4503513	Eukaryotic translation initiation factor3 subunit I	Q13347	Hs.530096	ED73I	20	7	5.38	36,878	301
5	gil9845502	40S ribosomal protein SA	P08865	Hs.449909	RPSA	42	16	4.79	32,947	914
6	gil306875	C protein	P07910	Hs.508848	HNRNP C	24	12	5.1	32,004	469
7	gll41327741	Protein ETHE1, mitochondrial precursor	095571	Hs.7486	ETHE1	14	3	6.35	28,368	140

were identified by LC–MS/MS; images of spots representing putative SET/TAF-Iβ interactors have been magnified (Fig. 2b). We identified X-ray repair cross-complementing protein 5 (XRCC5), also known as Ku80, among the interacting proteins (Table 1). The Ku70/80 heterodimeric complex has been reported to be closely involved in

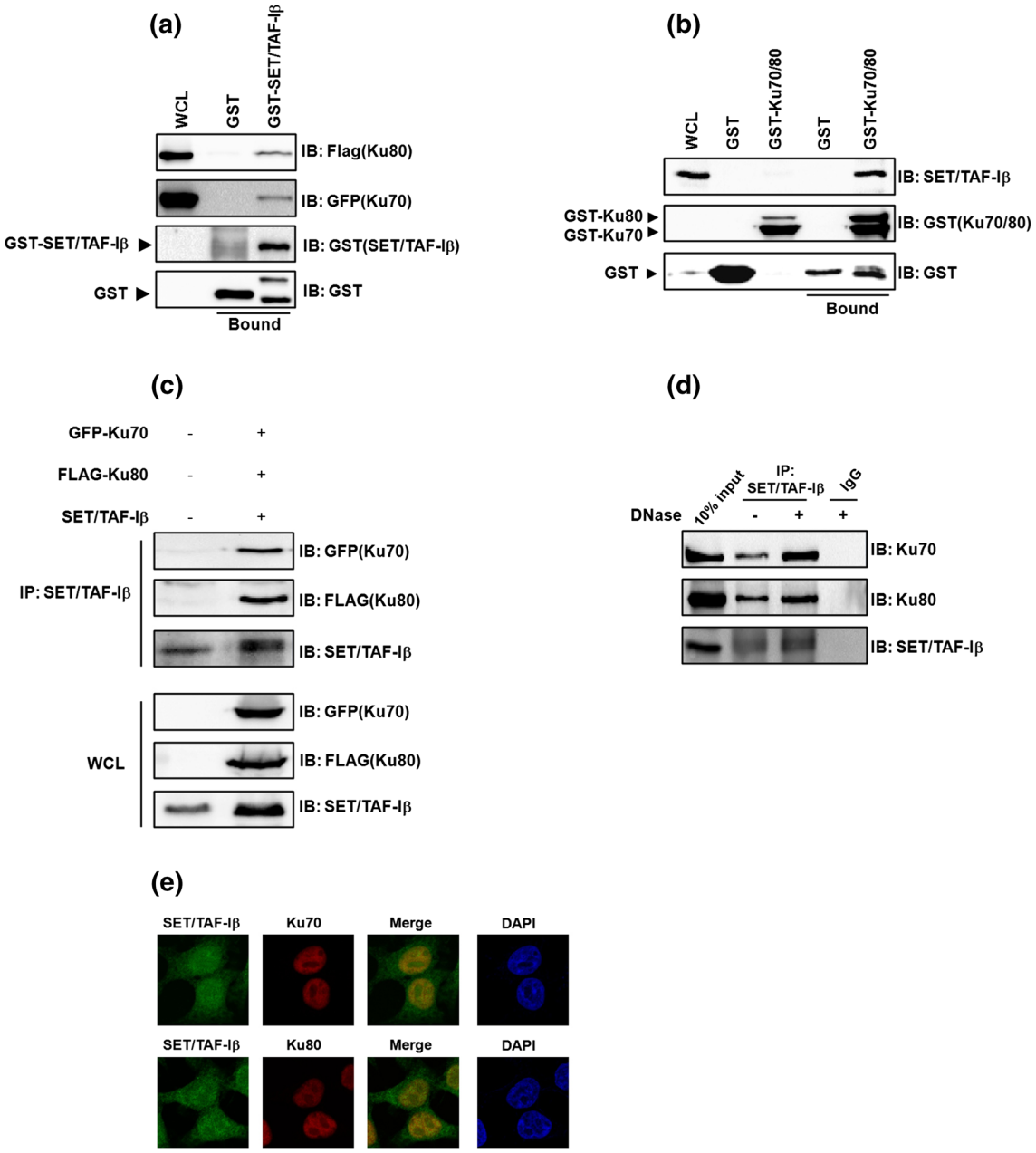

Fig. 3 SET/TAF-Iβ interacts with Ku70/80 both in vitro and in vivo. **a** 293T cells were transfected with constructs driving the expression of GFP-Ku70 and Flag-Ku80. Cell lysates were incubated with GST-SET/TAF-Iβ, and eluates were subsequently immunoblotted with anti-GST, anti-GFP, and anti-Flag antibodies. **b** 293T cells were transfected with a construct driving the expression of SET/TAF-Iβ. Cell lysates were incubated with recombinantly purified GST-Ku70/80; eluates were subsequently immunoblotted with anti-SET/TAF-Iβ and anti-GST antibodies. **c** 293T cells were co-transfected with constructs driving the expression of GFP-Ku70, Flag-Ku80, and SET/TAF-Iβ as indicated, and SET/TAF-Iβ immunoprecipitates were analyzed via immunoblotting with anti-GFP, anti-Flag, and anti-SET/TAF-Iβ antibodies. **d** 293T cell lysates were treated with DNase prior to immunoprecipitations with anti-SET/TAF-Iβ antibodies and control IgG antibodies. Immunoblot analysis of eluted proteins was then performed with anti-Ku70, anti-Ku80, and anti-SET/TAF-Iβ antibodies. **e** 293T cells were fixed, permeabilized, and immunostained with anti-Ku70, anti-Ku80, and anti-SET/TAF-Iβ antibodies. Nuclei were counterstained with DAPI

nonhomologous end-joining (NHEJ) after double-stranded breakage of DNA [20, 21]. In addition to these reports, recent studies have also demonstrated that histone modification by HATs or HDACs has an important effect on chromatin remodeling at DSB sites [19, 22, 23]. Therefore, we focused on the SET/TAF-Iβ-Ku80 interaction, with the aim of clarifying its function in DNA repair.

Interaction of SET/TAF-Iβ and Ku70/80

We next investigated whether SET/TAF-Iβ interacts with Ku70/80 by incubating lysates from cells ectopically expressing both GFP-Ku70 and Flag-Ku80 with purified GST-SET/TAF-Iβ. These experiments revealed a strong interaction between SET/TAF-Iβ and Ku70/80 (Fig. 3a). We confirmed this interaction by performing the experiment in reverse; that is, lysates from cells ectopically expressing SET/TAF-Iβ were incubated with GST-tagged, recombinant Ku70 and Ku80 (Fig. 3b). The interaction between SET/TAF-Iβ and Ku70/80 was also confirmed in vivo. SET/TAF-Iβ was immunoprecipitated with anti-SET/TAF-Iβ antibodies from lysates of cells ectopically expressing GFP-Ku70, Flag-Ku80, and SET/TAF-Iβ, and the presence of GFP-Ku70 and Flag-Ku80 in the eluate was confirmed by Western-blot analysis (Fig. 3c). We next investigated whether Ku70 interacts directly with SET/TAF-Iβ. In support of a direct interaction, in vitro transcribed and -translated Ku70 was retained on immobilized GST-SET/TAF-Iβ in in vitro pull down assays (Supplementary Fig. S2). To analyze the contribution of DNA toward this interaction, we included DNase in immunoprecipitations of endogenous SET/TAF-Iβ. These experiments revealed that the SET/TAF-Iβ-Ku70/80 interaction is not DNA-mediated, since Western blotting with anti-Ku70/80 antibodies of the immunoprecipitated proteins clearly indicated that the Ku70/80 heterodimer associates with SET/TAF-Iβ in a DNase-independent manner (Fig. 3d). Next, we investigated the subcellular localizations of endogenous SET/TAF-Iβ and Ku70/80. SET/TAF-Iβ was found predominantly in the nucleus, with some cytoplasmic distribution; similarly, both Ku70/80 proteins mainly localized to the nucleus (Fig. 3e). Together, these results indicate that SET/TAF-Iβ and Ku70/80 interact in vivo, this interaction is direct, and this interaction likely occurs in the nucleus.

Domain mapping of the Ku70 and SET/TAF-Iβ interaction

Given that SET/TAF-Iβ interacts with Ku70 and inhibits its acetylation, we next performed domain mapping of the SET/TAF-Iβ and Ku70 interaction. In vitro pull-down assays were performed with purified GST-SET/TAF-Iβ as bait, with preys GFP-Ku70 and Flag-Ku80 provided by cell extracts from transfected cells. Both Ku70 and Ku80 bound strongly to full-length SET/TAF-Iβ, but not to a version lacking the entire INHAT domain (SET/TAF-IβΔC5) (Fig. 4a). The domains involved in the in vivo interaction between SET/TAF-Iβ and Ku70/80 were confirmed by immunoprecipitation with anti-SET/TAF-Iβ antibodies, using cell extracts from transfected cells (Fig. 4b). Consistent with our pull-down data, SET/TAF-IβΔC5 (lacking the INHAT domain) and Ku70 did not interact at any detectable level. A weak interaction between SET/TAF-IβΔC5 and Ku80 was observed; this finding is probably due to the presence of endogenous SET/TAF-Iβ in the lysates, indicating the importance of the INHAT domain in the interaction (Fig. 4b). Interestingly, the GST-SET/TAF-Iβ (100–277) deletion mutant, containing an intact INHAT domain, interacted strongly with Ku70 and Ku80, indicating that binding is mediated by the C-terminal INHAT domain of SET/TAF-Iβ (Fig. 4a, b). To identify the domain(s) of Ku70 involved in the interaction, we performed the same set of in vitro and in vivo interaction assays with Ku70 deletion mutants. These assays indicated that the C-terminal region of Ku70, which contains both the nuclear localization signal (NLS) and residues known to be important for its interaction with Bax, also mediates its interaction with SET/TAF-Iβ (Fig. 4c). In vivo interactions were mapped further through immunoprecipitations performed with anti-HA antibodies from cell extracts of cells expressing various deletion mutants of Ku70. These experiments revealed that SET/TAF-Iβ bound strongly to the C-terminal region of Ku70

Fig. 4 SET/TAF-Iβ interaction with Ku70 is mediated by its INHAT ▶ domain. **a** Cell lysates from 293T cells ectopically expressing GFP-Ku70 and Flag-Ku80 were incubated with either GST-SET/TAF-Iβ, GST-SET/TAF-IβΔC5, or GST-SET/TAF-Iβ (100–277). Associated proteins were eluted, resolved by SDS-PAGE, and immunoblotted with anti-GFP and anti-Flag antibodies. The amounts of full-length SET/TAF-Iβ and SET/TAF-Iβ deletion mutants were determined by Coomassie staining. **b** 293T cells were transfected with constructs driving the expression of GFP-Ku70, Flag-Ku80, SET/TAF-Iβ, and SET/TAF-IβΔC5 prior to immunoprecipitation with anti-SET/TAF-Iβ antibodies. Associated proteins were eluted, resolved by SDS-PAGE, and immunoblotted with the indicated antibodies. The expression levels of SET/TAF-Iβ deletions were also determined by Western blotting (*lower panel*). **c** SET/TAF-Iβ was overexpressed in 293T cells prior to cell lysis and pull-down assays with immobilized GST-Ku70 deletion mutants as indicated. Associated proteins were eluted, resolved by SDS-PAGE, and immunoblotted with anti-SET/TAF-Iβ antibodies. The amounts of full-length Ku70 and Ku70 deletions were determined by Coomassie staining. **d** 293T cells were transfected with plasmids driving the expression of full-length HA-Ku70, deletion mutants thereof, and SET/TAF-Iβ prior to immunoprecipitations with anti-HA antibodies. Immunoprecipitated and associated proteins were eluted, resolved by SDS-PAGE, and immunoblotted with anti-HA and anti-SET/TAF-Iβ antibodies. The expression levels of Ku70 deletion proteins were determined by Western blotting (*lower panel*)

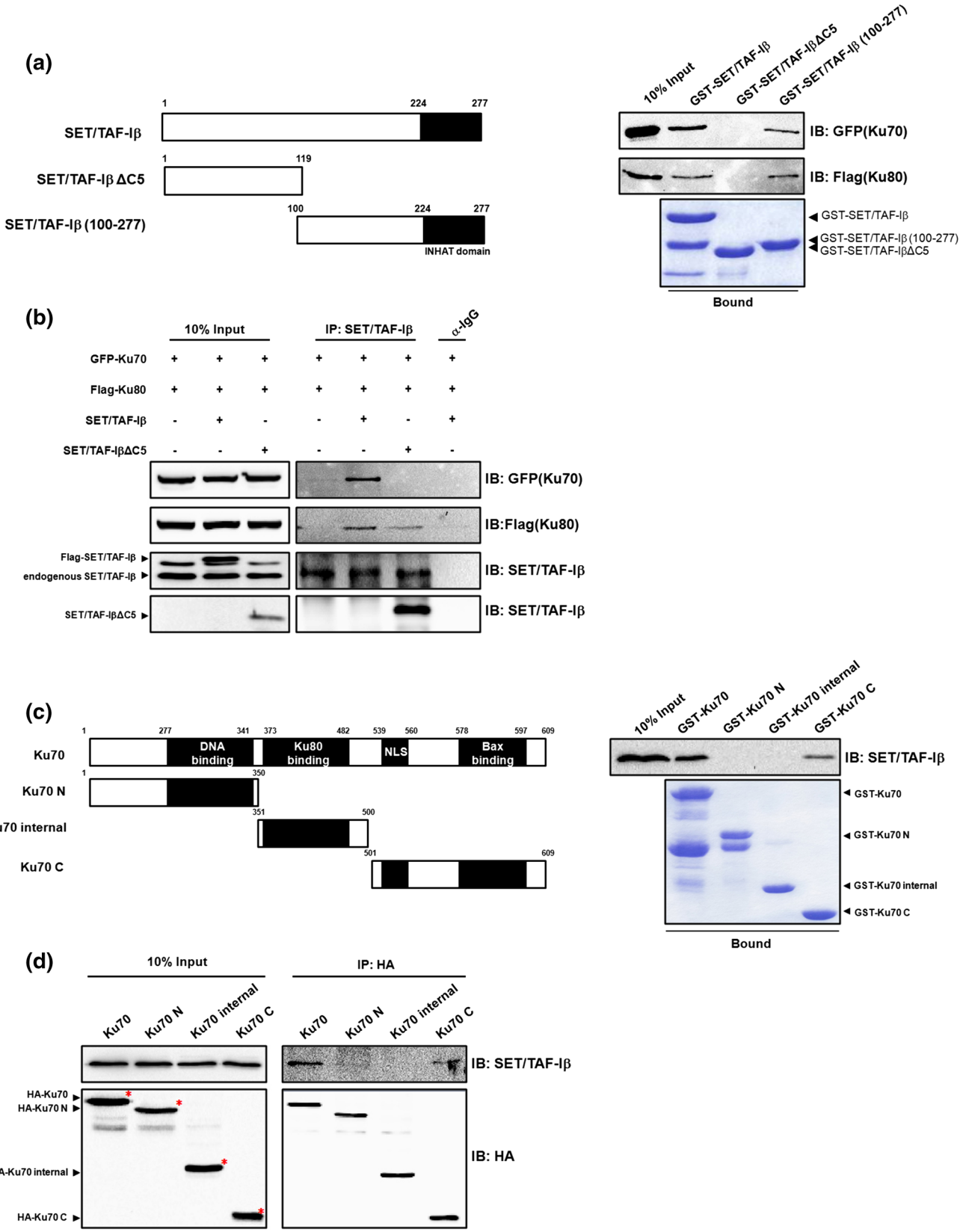
(a)
SET/TAF-Iβ
SET/TAF-Iβ ΔC5
SET/TAF-Iβ (100-277)
INHAT domain
10% Input
GST-SET/TAF-Iβ
GST-SET/TAF-IβΔC5
GST-SET/TAF-Iβ (100-277)
IB: GFP(Ku70)
IB: Flag(Ku80)
GST-SET/TAF-Iβ
GST-SET/TAF-Iβ (100-277)
GST-SET/TAF-IβΔC5
Bound
(b)
10% Input
IP: SET/TAF-Iβ
α-IgG
GFP-Ku70
Flag-Ku80
SET/TAF-Iβ
SET/TAF-IβΔC5
IB: GFP(Ku70)
IB:Flag(Ku80)
Flag-SET/TAF-Iβ
endogenous SET/TAF-Iβ
IB: SET/TAF-Iβ
SET/TAF-IβΔC5
IB: SET/TAF-Iβ
(c)
Ku70
DNA binding
Ku80 binding
NLS
Bax binding
Ku70 N
Ku70 internal
Ku70 C
10% Input
GST-Ku70
GST-Ku70 N
GST-Ku70 internal
GST-Ku70 C
IB: SET/TAF-Iβ
GST-Ku70
GST-Ku70 N
GST-Ku70 internal
GST-Ku70 C
Bound
(d)
10% Input
IP: HA
Ku70
Ku70 N
Ku70 internal
Ku70 C
IB: SET/TAF-Iβ
HA-Ku70
HA-Ku70 N
HA-Ku70 internal
HA-Ku70 C
IB: HA

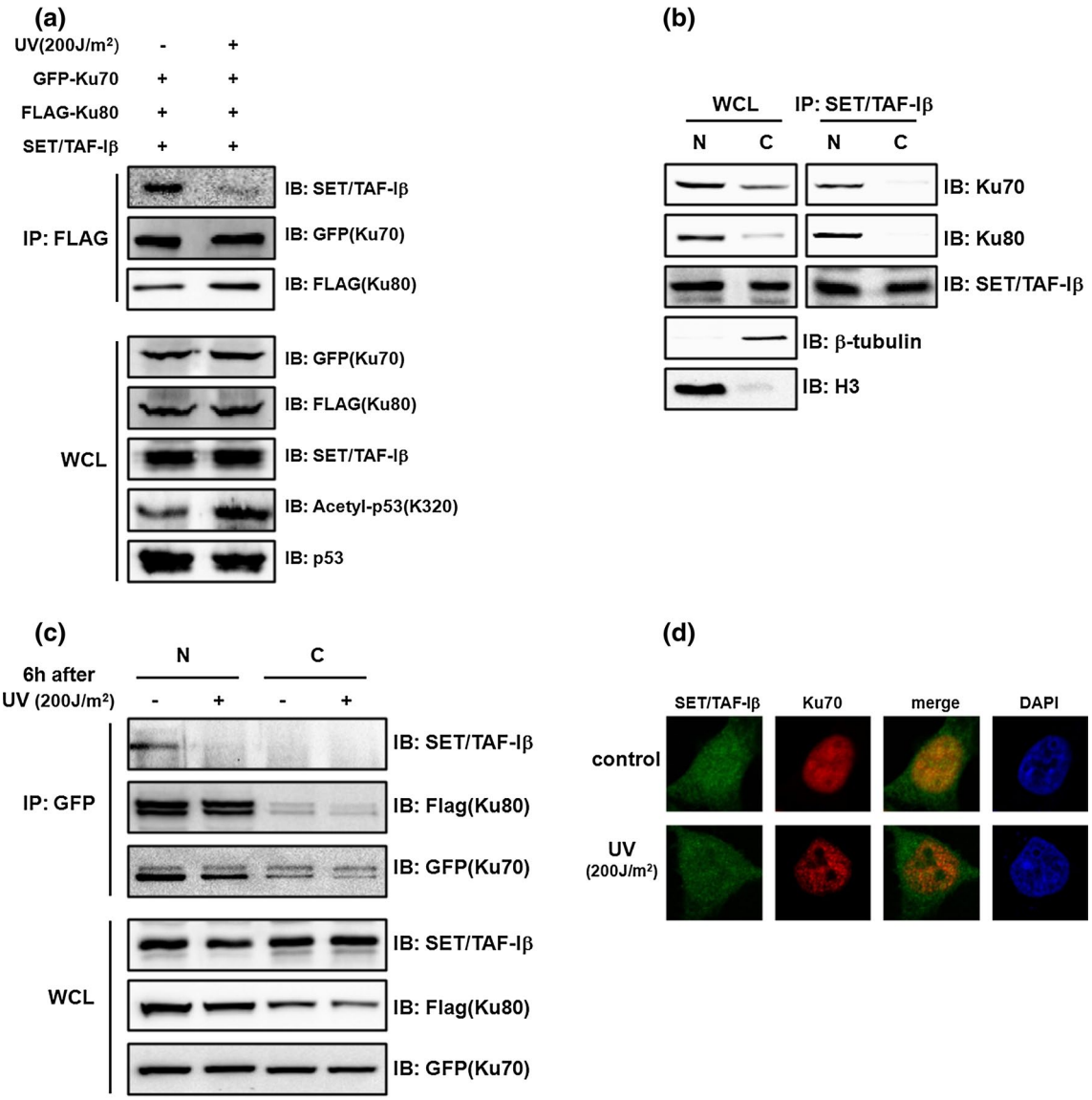

Fig. 5 The interaction between SET/TAF-Iβ and Ku70 is disrupted by UV-mediated DNA damage. **a** 293T cells were either untreated or treated with UV radiation (200 J/m^2). Ku80 was immunoprecipitated from lysates of 293T cells. Proteins present in immunoprecipitation inputs and eluates, including associated Ku80, were analyzed by Western blotting with the indicated antibodies. **b** SET/TAF-Iβ was immunoprecipitated from nuclear (N) and cytosolic (C) extracts with anti-SET/TAF-Iβ antibodies. Proteins present in eluates were resolved by SDS-PAGE and immunoblotted with anti-Ku70, anti-Ku80, and anti-SET/TAF-Iβ antibodies. **c** 293T cells ectopically expressing Ku70/80 and SET/TAF-Iβ were either untreated or treated with UV radiation (200 J/m^2). Cells were then fractionated to generate nuclear and cytosolic fractions. Finally, immunoprecipitations were performed from each extract with anti-GFP antibodies. **d** 293T cells were UV-irradiated (200 J/m^2). At 6-h post-irradiation, cells were fixed and immunostained with anti-SET/TAF-Iβ, and anti-Ku70 antibodies. Nuclei were counterstained with DAPI

(Fig. 4d). Consistent with the results shown in Fig. 1h, i, SET/TAF-Iβ bound to the C-terminal domain of Ku70, a region including its NLS and also possessing three acetylation sites (K539, K542, and K544). Therefore, we conclude that the SET/TAF-Iβ INHAT domain specifically interacts with the C-terminal domain of Ku70, and speculate that this interaction inhibits Ku70 acetylation by masking Ku70 from HATs.

DNA damage disrupts the Ku70-SET/TAF-Iβ interaction

Binding of Ku70/80 to both ends of broken DNA molecules occurs early in the process of NHEJ. To obtain further insight into the role of SET/TAF-Iβ in the Ku-mediated damage response to DSBs, we tested whether the interaction between SET/TAF-Iβ and Ku70/80 is affected by DNA damage. 293T cells were exposed to UV radiation,

and the interaction between SET/TAF-Iβ and Ku70/80 was monitored by immunoprecipitation and immunoblotting. These experiments revealed that the interaction between SET/TAF-Iβ and Ku70/80 was abrogated by UV damage (Fig. 5a). Importantly, the protein levels of Ku70/80 and SET/TAF-Iβ were not altered by UV damage (Fig. 5a). Cellular stresses, including DNA damage-induced acetylation of p53 at multiple C-terminal sites by p300/CBP and PCAF, are known to activate p53 [24]. Acetylation of p53 on residue K320 is indicative of stress-induced DNA damage (Fig. 5a). As a complementary approach, we treated cells with etoposide to mimic irradiation and investigated whether Ku70 and SET/TAF-Iβ underwent DNA damage-dependent dissociation (Supplementary Fig. 3). SET/TAF-Iβ dissociated from Ku70/80 upon treatment of 293T cells with etoposide, a result consistent with the data presented in Fig. 5a. Next, we examined whether the SET/TAF-Iβ-Ku70/80 interaction is localization-dependent. We began by detecting the localization of SET/TAF-Iβ in various cell lines. As expected, SET/TAF-Iβ was predominantly detected in the nucleus and also detected in the cytosol, albeit to a lesser extent (Fig. 5b). Consistent with a previous study, the DNA repair protein Ku70 was also predominantly localized in the nucleus (Fig. 5b). Intriguingly, immunoprecipitation of SET/TAF-Iβ from both nuclear and cytosolic extracts revealed that the SET/TAF-Iβ-Ku70/80 interaction appears to only occur in the nucleus (Fig. 5b). The reason for this compartmentalization of the Ku70 interaction is not currently known. To determine whether interactions between nuclear SET/TAF-Iβ and Ku proteins are affected by DNA damage, these interactions were examined by immunoprecipitation analysis. Surprisingly, DNA damage caused SET/TAF-Iβ to dissociate from Ku70, as determined by immunoprecipitations from nuclear extracts (Fig. 5c). Furthermore, the lack of interaction between cytosolic SET/TAF-Iβ and Ku70/80 was not altered by UV damage (Fig. 5c). As a complementary technique to confirm the dissociation of Ku-SET/TAF-Iβ binding upon DNA damage, we monitored the localizations of these proteins by confocal microscopy. We began by observing their localizations prior to UV irradiation and found that Ku70 and SET/TAF-Iβ colocalized in the nucleus (Fig. 5d). Consistent with the biochemical fractionation results, the localization of SET/TAF-Iβ did not change upon UV irradiation. In contrast, the localization of Ku70 shifted dramatically upon UV irradiation, forming distinct punctate structures in areas we speculate may represent double-strand break sites (Fig. 5d). Importantly, Ku70 and SET/TAF-Iβ failed to colocalize after UV irradiation, indicating that the Ku-SET/TAF-Iβ complex was dissociated by DNA damage (Fig. 5d). We then investigated the localization of SET/TAF-Iβ upon UV-mediated DNA damage through a subcellular fractionation approach. These experiments demonstrated that SET/TAF-Iβ did not change localization upon UV exposure (Supplementary Fig. 4a). To assess the amount of DNA damage induced in our experiments, we monitored the phosphorylation levels of histone H2AX (phospho-H2AX) as a proxy measurement of DNA damage (Supplementary Fig. 4a) [25]. In addition, the expression levels of Ku70/80 were monitored and found to be unchanged in the presence and absence of DNA damage (data not shown). To determine whether the ubiquitin–proteasome pathway is involved in the DNA damage-dependent dissociation of Ku70/80 and SET/TAF-Iβ, we performed ubiquitination assays with SET/TAF-Iβ and Ku70/80 in the presence of the 26S proteasome inhibitor, MG132. In our assay conditions, these experiments did not provide any indication that ubiquitination of either SET/TAF-Iβ or Ku70/80 both in the absence and presence of UV irradiation (Supplementary Fig. 4b). Together, these results provide strong evidence that SET/TAF-Iβ and Ku70/80 binding is dissociated upon UV-mediated DNA damage.

SET/TAF-Iβ inhibits recruitment of Ku70/80 to DNA damage sites

To determine whether SET/TAF-Iβ-mediated inhibition of Ku70 acetylation is of biological significance, we analyzed the effects of SET/TAF-Iβ on NHEJ repair activity. For this, we generated a 293TdA3 stable cell line harboring the pIRES-TK-EGFP plasmid integrated into the genomic DNA. This plasmid contains two recognition sites for *I-Sce*I endonuclease [19], which act as substrates for DSBs and subsequent NHEJ repair. In this system, the readout for NHEJ activity corresponds to the levels of C-terminally EGFP-tagged protein, which can only be produced if DSBs are ligated by NHEJ repair. Since acetylation of Ku70 was inhibited by the INHAT domain of SET/TAF-Iβ, we evaluated NHEJ repair activity in the presence of ectopically expressed full-length SET/TAF-Iβ and SET/TAF-IβΔC5. Upon overexpression of SET/TAF-Iβ, the level of EGFP fluorescence was significantly decreased compared to that of control cells (Fig. 6a). However, the level of EGFP fluorescence was significantly recovered upon expression of SET/TAF-IβΔC5 (Fig. 6a). More importantly, shRNA-mediated knockdown of endogenous SET/TAF-Iβ by two different sequences further increased EGFP fluorescence, thereby confirming the inhibitory effect of endogenous SET/TAF-Iβ on NHEJ repair (Fig. 6a). To further investigate the effects of SET/TAF-Iβ on NHEJ repair activity, we used real-time PCR to analyze whether SET/TAF-Iβ inhibits its NHEJ repair through regulation of Ku70 acetylation. These experiments showed that the proportion of joined DNA decreased, whereas that of uncut DNA remained unchanged, upon overexpression of SET/TAF-Iβ (Fig. 6b;

Supplementary Fig. 5a). In contrast, overexpression of SET/TAF-IβΔC5 had the opposite effect on the proportion of joined DNA, indicating the importance of the HAT inhibition domain of SET/TAF-Iβ on NHEJ repair. Consistent with the fluorescence data, shRNA-mediated knockdown of SET/TAF-Iβ by two different sequences significantly increased the proportions of joined DNA (Fig. 6b). To evaluate the proportions of joined DNA in each sample, we also performed real-time PCR using primers inside of joined DNA fragments as an internal control (Supplementary Fig. 5b). Since NHEJ repair activity was decreased by overexpression of SET/TAF-Iβ, we hypothesized that SET/TAF-Iβ inhibits Ku70 recruitment to DNA damage sites via regulation of Ku70 acetylation. To determine whether inhibition of Ku70 acetylation by the INHAT activity of SET/TAF-Iβ affects recruitment of Ku70/80 to DSB sites, we performed ChIP analysis with ectopically expressed SET/TAF-Iβ and SET/TAF-IβΔC5. The indicated regions, downstream of the second *I-Sce*I site in the pIRES-TK-EGFP plasmid sequence, were immunoprecipitated with anti-Flag (Ku80), anti-HA (Ku70), and anti-phospho-H2AX antibodies (Fig. 6c). For the 0.3-kb region, qPCR showed that enrichment of Ku70 and Ku80 was significantly decreased upon overexpression of SET/TAF-Iβ, but not of SET/TAF-IβΔC5 (Fig. 6c). These patterns were only detected for the 0.3-kb region, the region closest to the DSB site, and not for the 1.2- or 2.5-kb regions after *I-Sce*I digestion. The observation that SET/TAF-Iβ, but not SET/TAF-IβΔC5, negatively regulated Ku70/80 recruitment to DSB sites strongly suggests that inhibition of Ku70 acetylation by SET/TAF-Iβ plays a role in the Ku-mediated NHEJ repair pathway. Our findings collectively indicate that SET/TAF-Iβ inhibits recruitment of Ku70/80 to DNA damage sites and inhibits NHEJ repair through its INHAT activity. To further elucidate the biological function of SET/TAF-Iβ in the Ku70/80-mediated NHEJ repair pathway, we measured cell viability and proliferation. The effect of SET/TAF-Iβ on the viability of DSB-damaged cells was analyzed by counting the numbers of live cells upon SET/TAF-Iβ overexpression or knockdown, combined with etoposide treatment. Cells overexpressing SET/TAF-Iβ exhibited decreased viability (50 %) compared to that of control vector-transfected cells; furthermore, cell viability was recovered by shRNA-mediated knockdown of SET/TAF-Iβ by different sequences (Fig. 6d). BrdU incorporation assays also indicated that cellular proliferation is impeded by overexpression of SET/TAF-Iβ, most likely due to delayed recovery of DNA repair; proliferation was restored by shRNA-mediated knockdown of SET/TAF-Iβ by different sequences (Fig. 6e). The effects of SET/TAF-Iβ overexpression and knockdown were complementary, supporting the idea that SET/TAF-Iβ regulates the Ku70/80-mediated DNA repair pathway, at least in 293T cells treated with etoposide (Fig. 6e).

Fig. 6 SET/TAF-Iβ blocks Ku70 recruitment to DSB sites upon UV-mediated DNA damage. **a**, **b** The amounts of **a** EGFP-positive cells and **b** joined DNA observed upon overexpression of SET/TAF-Iβ, SET/TAF-IβΔC5, and shRNA-mediated silencing of SET/TAF-Iβ are expressed as proportions of the amounts observed after transfection with empty vector. Data are expressed as mean values from three independent experiments ± SDs. Results from immunoblot analysis are shown on the right in **a**. β-actin was used as a loading control. Data shown represent averages of three independent experiments, with error bars representing ± SDs. * $p < 0.05$, ** $p < 0.01$; *** $p < 0.001$ compared with control cells. **c** Primer sites used for quantitative PCR are shown at the top, including the distances between primer and I-*Sce*I sites. ChIP was performed with either control immunoglobulin G, or antibodies against phospho-H2AX, Flag, HA, and SET/TAF-Iβ, 48 h after transfection of the I-*Sce*I expression plasmid into 293T cells. Relative enrichments of proteins after 48 h (compared with 0 h) are shown. **d** Cell viability was determined by the MTT assay. 293T cells were treated with etoposide (5 μM) and transfected with the indicated constructs. Results are shown as means ± SDs; $n = 3$. ** $p < 0.01$; *** $p < 0.001$ compared with untreated cells. **e** 293T cells were transfected with the indicated constructs after treatment with etoposide (5 μM). At 72-h post-transfection, cells were fixed and BrdU assays performed. Results shown represent means ± SDs; $n = 3$. ** $p < 0.01$; *** $p < 0.001$. **f** Proposed model of how SET/TAF-Iβ regulates Ku70/80-mediated DSB DNA repair via inhibition of Ku70 acetylation

Discussion

In this study, we report that the Ku70/80 heterodimer, involved in NHEJ, interacts with SET/TAF-Iβ. Importantly, we also demonstrate for the first time that Ku70 acetylation can be inhibited by SET/TAF-Iβ. The interaction between SET/TAF-Iβ and Ku70/80 is abrogated by DNA damage; we hypothesize that the dissociated Ku70/80 can be recruited to DSB sites for further repair. We also showed that SET/TAF-Iβ-mediated inhibition of Ku70 acetylation requires the C-terminus of the SET/TAF-Iβ INHAT domain. Our data favor a model in which SET/TAF-Iβ negatively regulates Ku70/80 recruitment to DSB sites, thereby slowing the DNA damage repair process.

Initially identified as a DNA DSB-repairing protein, Ku70 can be acetylated by both CBP and PCAF, thereby inducing Bax-mediated apoptosis. Interestingly, HDAC inhibitors have been shown to sensitize prostate cancer cells to DNA DSB-producing agents by targeting Ku70 acetylation [6]. Furthermore, SIRT1 has been shown to promote the ability of Ku70 to inhibit Bax-mediated apoptosis by sequestering Bax away from mitochondria during calorie restriction [4].

A number of studies have established a connection between histone acetylation and transcriptional regulation [26, 27]. Furthermore, several non-histone proteins have been shown to be acetylated by various HATs, with physiologically relevant consequences [28]. We have previously demonstrated that the proto-oncogene protein, SET/TAF-Iβ, inhibits p300- and PCAF-mediated p53

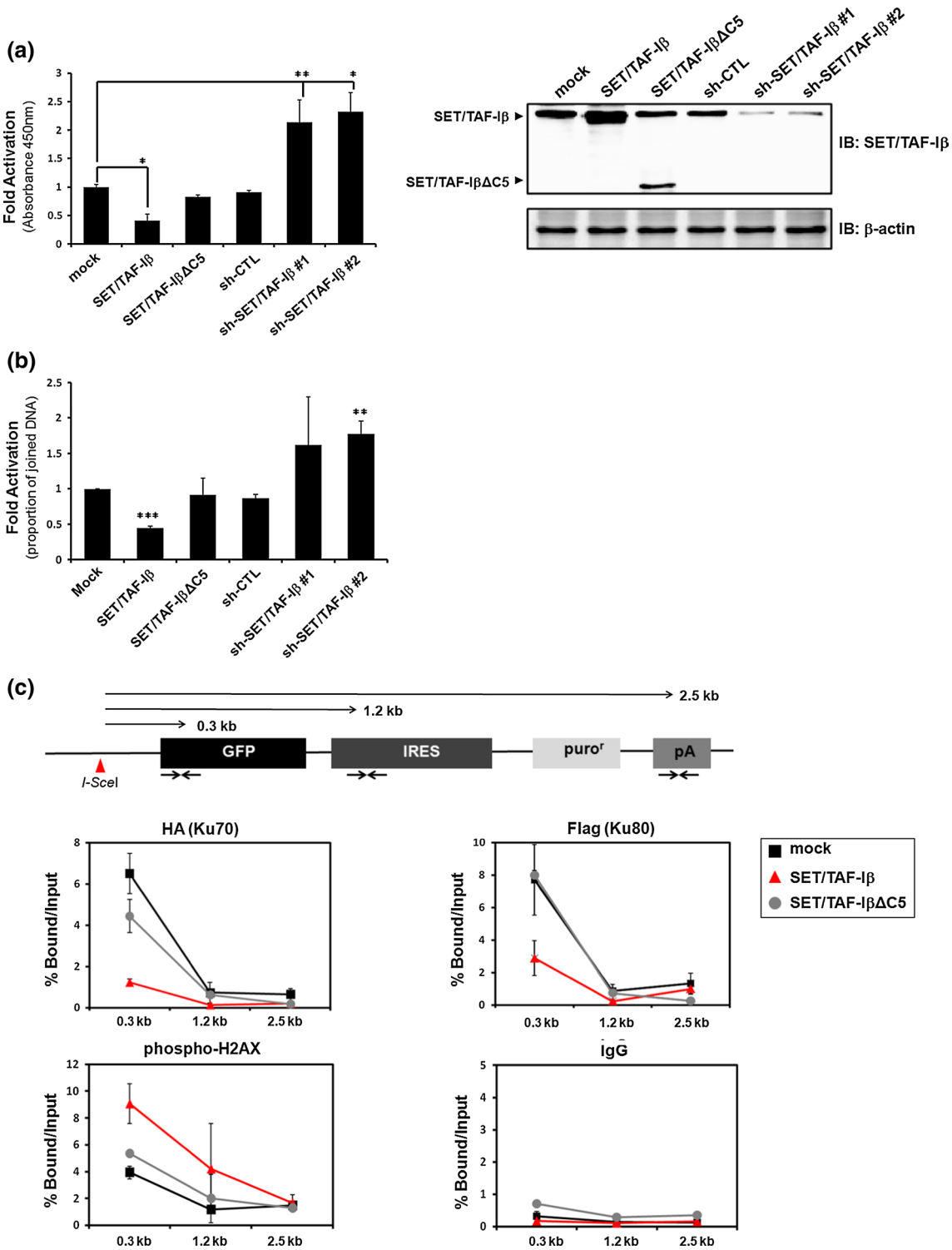

acetylation and negatively regulates p53 activity [15]. It has also been suggested that SET/TAF-Iβ induces cell cycle arrest upon cellular stress by inhibiting p53 acetylation. Our data support the idea that SET/TAF-Iβ prevents repair of DNA DSBs by inhibiting Ku70/80 recruitment, thereby causing the accumulation of damaged DNA inside cells and eventually leading to cellular proliferation and carcinogenesis. Consistent with this hypothesis, SET/TAF-Iβ-regulated recruitment of the non-histone acetylation substrates, p53 and Ku70, to target promoter and DSB sites, respectively, was mediated by interaction with the HAT inhibitory domain.

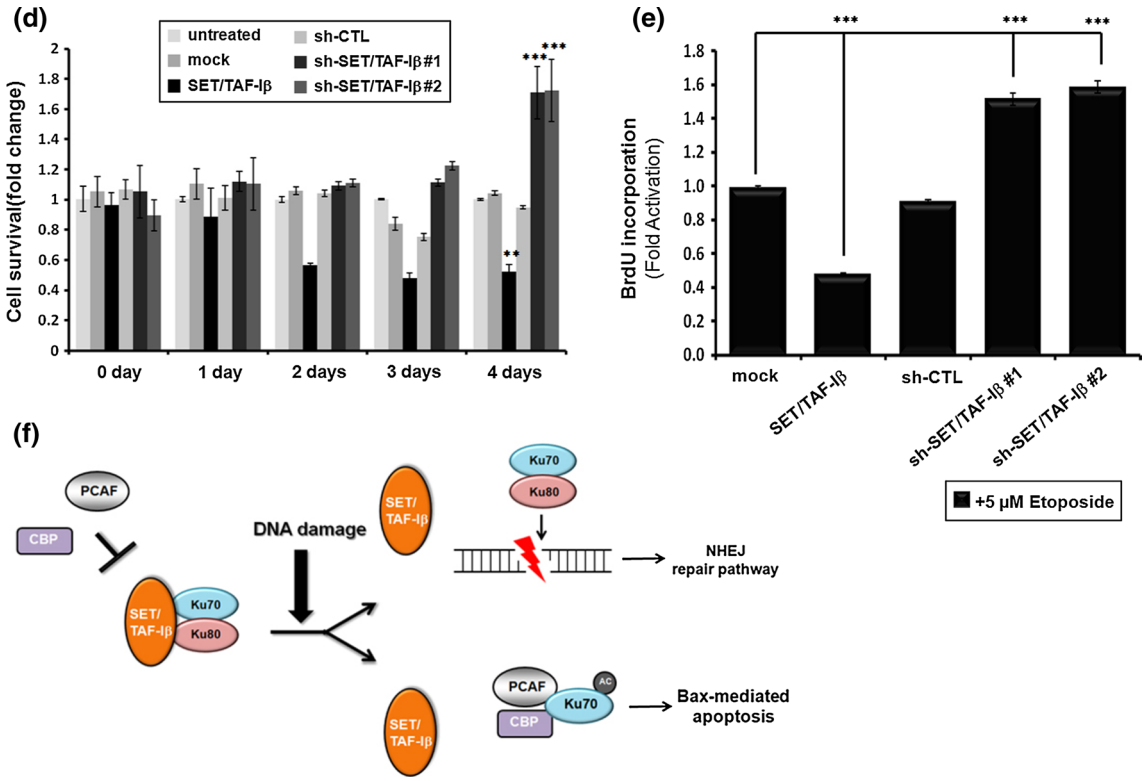

Fig. 6 continued

In conclusion, our data provide evidence that SET/TAF-Iβ is involved in the NHEJ DNA repair pathway through interaction with Ku70/Ku80; furthermore, this interaction was demonstrated at physiological concentrations. Our results support a model in which SET/TAF-Iβ inhibits Ku proteins from either being recruited to DNA DSBs, or being acetylated by HATs, via inhibition of Ku70 acetylation via its INHAT domain in the absence of DNA damage. Once DNA DSBs are induced, SET/TAF-Iβ dissociates from Ku70/80, leaving Ku70/80 free to bind to the ends of broken DNA. We propose the following model for the regulation of Ku70 acetylation by SET/TAF-Iβ: Under normal conditions, SET/TAF-Iβ interacts with Ku70/80 in the nucleus. This interaction is mediated by the INHAT domain of SET/TAF-Iβ and the C-terminal region of Ku70. Upon DNA damage, SET/TAF-Iβ dissociates from the Ku complex, thereby allowing these proteins to be recruited to DNA DSB sites. However, upon SET/TAF-Iβ overexpression, the normal association and dissociation patterns of SET/TAF-Iβ and Ku proteins are disrupted, leading to inhibition of both NHEJ DNA repair and Ku70 acetylation-mediated apoptosis (Fig. 6f). Importantly, our study indicates that dysregulation of SET/TAF-Iβ expression may result in serious consequences to the NHEJ DNA repair process. This model is consistent with previous studies of the oncogenic aspects of SET/TAF-Iβ, mediated by its INHAT activity [15]. Consistent with our model, SET/TAF-Iβ sensitized cells to the DNA-damaging agent, etoposide, by delaying DNA repair and decreasing cellular viability and proliferation. Additional investigations into the mechanism of dissociation between Ku proteins and SET/TAF-Iβ upon DNA damage should provide important information about the regulation of this important interaction. The results described in this study add another layer of complexity to the INHAT subunit of SET/TAF-Iβ, already known to play an important role in acetylation-mediated inhibition of histones and non-histone proteins by HATs. This study describes a role for the INHAT subunit that is not on the transcriptional level; rather, the INHAT subunit also plays a role in the DNA repair pathway. Further investigation will aim to increase our understanding of the diverse roles of the multifunctional protein, SET/TAF-Iβ, in controlling multiple aspects of cellular physiology.

Acknowledgments We thank Dr. Takashi Kohno of the National Cancer Center Research Institute for the pIRES-TK-EGFP plasmid and Dr. Maria Jasin of the Memorial Sloan-Kettering Cancer Center for the pCBASce plasmid. This work was supported by the Ministry of Education, Science and Technology (2009-0073484), the Basic Science Research program through the National Research Foundation of Korea (NRF), and the Next-Generation BioGreen 21 Program (PJ008116062011), Rural Development Administration, Republic of Korea.

References

1. Hoeijmakers JH (2001) Genome maintenance mechanisms for preventing cancer. Nature 411(6835):366–374
2. Wyman C, Kanaar R (2006) DNA double-strand break repair: all's well that ends well. Annu Rev Genet 40:363–383
3. Cohen HY, Lavu S, Bitterman KJ, Hekking B, Imahiyerobo TA, Miller C, Frye R, Ploegh H, Kessler BM, Sinclair DA (2004) Acetylation of the C terminus of Ku70 by CBP and PCAF controls Bax-mediated apoptosis. Mol Cell 13(5):627–638
4. Cohen HY, Miller C, Bitterman KJ, Wall NR, Hekking B, Kessler B, Howitz KT, Gorospe M, de Cabo R, Sinclair DA (2004) Calorie restriction promotes mammalian cell survival by inducing the SIRT1 deacetylase. Science 305(5682):390–392
5. Subramanian C, Opipari AW Jr, Bian X, Castle VP, Kwok RP (2005) Ku70 acetylation mediates neuroblastoma cell death induced by histone deacetylase inhibitors. Proc Natl Acad Sci USA 102(13):4842–4847
6. Chen CS, Wang YC, Yang HC, Huang PH, Kulp SK, Yang CC, Lu YS, Matsuyama S, Chen CY (2007) Histone deacetylase inhibitors sensitize prostate cancer cells to agents that produce DNA double-strand breaks by targeting Ku70 acetylation. Cancer Res 67(11):5318–5327
7. Seo SB, Macfarlan T, McNamara P, Hong R, Mukai Y, Heo S, Chakravarti D (2002) Regulation of histone acetylation and transcription by nuclear protein pp32, a subunit of the INHAT complex. J Biol Chem 277(16):14005–14010
8. Seo SB, McNamara P, Heo S, Turner A, Lane WS, Chakravarti D (2001) Regulation of histone acetylation and transcription by INHAT, a human cellular complex containing the set oncoprotein. Cell 104(1):119–130
9. Chakravarti D, Hong R (2003) SET-ting the stage for life and death. Cell 112(5):589–591
10. Fan Z, Beresford PJ, Oh DY, Zhang D, Lieberman J (2003) Tumor suppressor NM23-H1 is a granzyme A-activated DNase during CTL-mediated apoptosis, and the nucleosome assembly protein SET is its inhibitor. Cell 112(5):659–672
11. Jiang X, Kim HE, Shu H, Zhao Y, Zhang H, Kofron J, Donnelly J, Burns D, Ng SC, Rosenberg S, Wang X (2003) Distinctive roles of PHAP proteins and prothymosin-alpha in a death regulatory pathway. Science 299(5604):223–226
12. Adachi Y, Pavlakis GN, Copeland TD (1994) Identification and characterization of SET, a nuclear phosphoprotein encoded by the translocation break point in acute undifferentiated leukemia. J Biol Chem 269(3):2258–2262
13. Nagata K, Kawase H, Handa H, Yano K, Yamasaki M, Ishimi Y, Okuda A, Kikuchi A, Matsumoto K (1995) Replication factor encoded by a putative oncogene, set, associated with myeloid leukemogenesis. Proc Natl Acad Sci USA 92(10):4279–4283
14. von Lindern M, van Baal S, Wiegant J, Raap A, Hagemeijer A, Grosveld G (1992) Can, a putative oncogene associated with myeloid leukemogenesis, may be activated by fusion of its 3′ half to different genes: characterization of the set gene. Mol Cell Biol 12(8):3346–3355
15. Kim JY, Lee KS, Seol JE, Yu K, Chakravarti D, Seo SB (2012) Inhibition of p53 acetylation by INHAT subunit SET/TAF-Ibeta represses p53 activity. Nucleic Acids Res 40(1):75–87
16. Chae JI, Kim J, Lee SG, Koh MW, Jeon YJ, Kim DW, Ko SM, Seo KS, Lee HK, Choi NJ, Cho SK, Ryu J, Kang S, Lee DS, Chung HM, Koo DB (2012) Quantitative proteomic analysis of pregnancy-related proteins from peripheral blood mononuclear cells during pregnancy in pigs. Anim Reprod Sci 134(3–4):164–176
17. Zuo X, Echan L, Hembach P, Tang HY, Speicher KD, Santoli D, Speicher DW (2001) Towards global analysis of mammalian proteomes using sample pre-fractionation prior to narrow pH range two-dimensional gels and using one-dimensional gels for insoluble and large proteins. Electrophoresis 22(9):1603–1615
18. Knuesel M, Wan Y, Xiao Z, Holinger E, Lowe N, Wang W, Liu X (2003) Identification of novel protein-protein interactions using a versatile mammalian tandem affinity purification expression system. Mol Cell Proteomics 2(11):1225–1233
19. Ogiwara H, Ui A, Otsuka A, Satoh H, Yokomi I, Nakajima S, Yasui A, Yokota J, Kohno T (2011) Histone acetylation by CBP and p300 at double-strand break sites facilitates SWI/SNF chromatin remodeling and the recruitment of non-homologous end joining factors. Oncogene 30(18):2135–2146
20. Burma S, Chen BP, Chen DJ (2006) Role of non-homologous end joining (NHEJ) in maintaining genomic integrity. DNA Repair (Amst) 5(9–10):1042–1048
21. Lieber MR (2008) The mechanism of human nonhomologous DNA end joining. J Biol Chem 283(1):1–5
22. Das C, Lucia MS, Hansen KC, Tyler JK (2009) CBP/p300-mediated acetylation of histone H3 on lysine 56. Nature 459(7243):113–117
23. Tjeertes JV, Miller KM, Jackson SP (2009) Screen for DNA-damage-responsive histone modifications identifies H3K9Ac and H3K56Ac in human cells. EMBO J 28(13):1878–1889
24. Avantaggiati ML, Ogryzko V, Gardner K, Giordano A, Levine AS, Kelly K (1997) Recruitment of p300/CBP in p53-dependent signal pathways. Cell 89(7):1175–1184
25. Taneja N, Davis M, Choy JS, Beckett MA, Singh R, Kron SJ, Weichselbaum RR (2004) Histone H2AX phosphorylation as a predictor of radiosensitivity and target for radiotherapy. J Biol Chem 279(3):2273–2280
26. Jenuwein T, Allis CD (2001) Translating the histone code. Science 293(5532):1074–1080
27. Strahl BD, Allis CD (2000) The language of covalent histone modifications. Nature 403(6765):41–45
28. Spange S, Wagner T, Heinzel T, Kramer OH (2009) Acetylation of non-histone proteins modulates cellular signalling at multiple levels. Int J Biochem Cell Biol 41(1):185–198